sustainability

MDPI

Article

Soil Water Retention and Pore Characteristics of Intact Loess Buried at Different Depths

Xiaokun Hou [1,2,*], Shengwen Qi [1,2] and Fangcui Liu [1,2]

[1] Key Laboratory of Shale Gas and Geoengineering, Institute of Geology and Geophysics, Chinese Academy of Sciences, Beijing 100029, China; qishengwen@mail.iggcas.ac.cn (S.Q.); fangcui@mail.iggcas.ac.cn (F.L.)
[2] Innovation Academy for Earth Sciences, Chinese Academy of Sciences (CAS), Beijing 100029, China
* Correspondence: xhou098@mail.iggcas.ac.cn

Abstract: Surface water infiltration is a primary factor responsible for engineering challenges and geological disasters on the Loess Plateau of China (LPC). Due to the extensive groundwater in this region, surface water must pass through thick unsaturated zones to recharge the groundwater reservoirs. Exploring the unsaturated hydraulic characteristics of loess, especially at varying depths, may significantly contribute to disaster prevention and mitigation and the pursuit of sustainable development in the Loess Plateau. The soil-water characteristic curve (SWCC), intricately linked to the soil's pore structure, is a critical hydraulic parameter of loess. An exploration well with a depth of 30 m was excavated in the LPC to obtain intact specimens at depths of 5 m, 15 m, and 25 m. Basic physical property tests, SWCC measurements, and particle size distribution (PSD) analyses were conducted. Additionally, the relationship between PSD and SWCC is discussed in this paper. The findings highlight the influence of depth on the dominant pore size and distribution density, both of which decreased with increasing depth. The air occlusion value of the SWCC experienced an increase, and the slope of the SWCC in the transition zone exhibited consistency. These observations underscore the pivotal role played by pore structure in shaping the soil's water-retention behavior. Furthermore, predictions based on PSD data demonstrated excellent accuracy in replicating the wetting SWCC of loess over a wide suction range (e.g., 10–10^4 kPa).

Keywords: Loess Plateau of China; intact loess; soil water retention curve; pore size distribution; buried depth

Citation: Hou, X.; Qi, S.; Liu, F. Soil Water Retention and Pore Characteristics of Intact Loess Buried at Different Depths. *Sustainability* **2023**, *15*, 14890. https://doi.org/10.3390/su152014890

Academic Editors: Alfrendo Satyanaga, Qian Zhai, Zhong Han, Arezoo Rahimi and Yunlong Liu

Received: 9 September 2023
Revised: 6 October 2023
Accepted: 11 October 2023
Published: 15 October 2023

1. Introduction

Loess soils are prevalent in semi-arid and arid regions across the globe, including countries such as China, Russia, and the USA. In China, these loess deposits date back approximately 2.4 million years (2.4 Ma), giving rise to the renowned Loess Plateau of China (CPL), which covers an expansive area of over 440,000 km^2 [1,2]. These soils typically exhibit an open structure characterized by a random arrangement of particles, high porosity, and a substantial presence of macro pores. These can be attributed to the prevalence of silt-sized particles in their composition and the aeolian origin of loess soils. For instance, in China, soil materials from the Gobi Desert have been transported by wind to the Loess Plateau.

Loess soils typically exist in an unsaturated state and are susceptible to volume reduction, known as collapse, upon exposure to moisture or external loading [3]. This inherent characteristic results in a significant reduction in their strength, consequently contributing to a range of disasters, including landslides and foundation failures. Notably, the infiltration of surface water serves as the primary trigger for engineering and geological disasters, such as collapsibility, landslides, and mudflows [4–7]. Due to the deep burial of groundwater in the loess area, surface water must pass through the thick unsaturated loess layer to recharge the groundwater [8–12]. Exploring the unsaturated hydraulic

characteristics of loess, especially the soil buried at varying depths, has the potential to significantly advance disaster prevention and mitigation efforts, ultimately fostering sustainable development across the CPL.

The soil water characteristic curve (SWCC), which depicts the relationship between soil water content (or degree of saturation) and suction, serves as a fundamental tool for understanding the behavior of hydraulic conductivity in unsaturated soils [13–15]. Many researchers have utilized the SWCC to predict unsaturated permeability coefficients [13,15–18]. These predictions are based on the inherent connection between the SWCC and microstructure, especially pore size distribution (PSD). Factors influencing the SWCC include soil type [19], stress history and stress state [20], density [16,17], soil structure [21,22], hydraulic path (i.e., drying or wetting) [23], and more. Among these factors, stress state, stress history, and density alter the SWCC by affecting the soil's structure.

Various SWCC functions have been proposed, including the typical unimodal SWCC functions by van Genuchten [18] and Fredlund and Xing [13], the bimodal SWRC functions by Otalvaro et al. [24], and the advanced functions that account for soil deformation proposed by Romero et al. [25] and Hu et al. [17], all grounded in soil PSD characteristics. Additionally, the choice of hydraulic path (i.e., drying or wetting) significantly influences soil water retention behavior, with the drying path typically resulting in higher water content or degree of saturation compared to the wetting path at the same suction value. This phenomenon is referred to as hysteresis [26].

Historically, previous investigations into soil water retention behavior have primarily focused on the drying path, where the soil is initially saturated before undergoing desaturation, or on the drying–wetting paths to examine hysteresis [23]. Furthermore, despite the increased interest in unsaturated soils over the past decades, relatively limited data on intact soils have been published [27,28]. It is worth acknowledging the existence of various studies focused on the SWCC of loess; however, most of these studies have prioritized compacted specimens, as obtaining intact specimens is both labor-intensive and costly. Consequently, the soil structures and SWCC characteristics of intact soil remain a subject requiring further exploration and understanding.

In this study, a 30 m deep well was excavated in Heping Town, Lanzhou City, Gansu Province to obtain intact samples at different depths (i.e., 5 m, 15 m, and 25 m). The SWCC for the loess samples was determined using a combination of the filter paper method and the axis translation technique. Furthermore, we conducted a comparative analysis to examine changes in the pore size distribution (PSD) curve for the loess samples at different depths. The PSD curve was essential for quantitatively elucidating the distinctive characteristics of the pore structure within the sampled layers. To enhance our understanding, we applied the Young–Laplace equation to convert pore sizes into corresponding suction values and overlaid the PSD and SWCC curves on the suction coordinate. This integrated approach allowed us to dissect and interpret the intricate interplay between the pore structure distribution of the loess and its SWCC. Ultimately, we conducted SWCC predictions using the pore data. The results emphasize the dominant role played by pore structure in governing the soil's capacity to retain water. The insights gained from this study make valuable contributions to our understanding of soil behavior under unsaturated conditions, particularly in loess formations subjected to varying burial depths.

2. Materials and Methods

2.1. Materials

A well 30 m in depth was excavated in Heping Town, Lanzhou City, Gansu Province, to obtain intact samples at different depths (i.e., 5, 15, and 25 m). These samples were carefully wrapped in plastic film and then placed inside wooden containers filled with sawdust to minimize potential disruption during transportation.

The basic physical characteristics of the samples are summarized in Table 1. The natural moisture content of the uppermost loess was lower when compared to the deeper layers. With increasing burial depth, several trends became evident: dry density increases,

porosity decreases, and saturation moisture content decreases. Importantly, the plastic limit index remained relatively stable regardless of burial depth.

Table 1. Basic physical properties of the specimens.

Samples	ρ_d (g/cm^3)	e	w (%)	L_L(%)	P_L (%)	PI	w_{sat} (%)
D = 5 m	1.35	1.0	7.6	26.1	18.5	7.6	37.0
D = 15 m	1.40	0.93	16.2	27.5	19.1	8.4	34.4
D = 25 m	1.45	0.86	17.9	27.8	20.1	7.7	31.9

Note: ρ_d is the dry density; e is the void ratio; w is the soil water content; L_L is the liquid limit; P_L is the plastic limit; PI is the plastic index; w_{sat} is the saturated water content.

The particle size distribution curves were determined using a laser particle size analyzer, as depicted in Figure 1. These curves generally followed a consistent trend. Fine particles in the range of 0.002 mm to 0.050 mm made up most of the loess, comprising about 60% to 75% of its composition. The clay fraction, with particles smaller than 0.002 mm, made up a smaller portion, around 5% to 10%. The sand fraction accounted for approximately 10% to 30%.

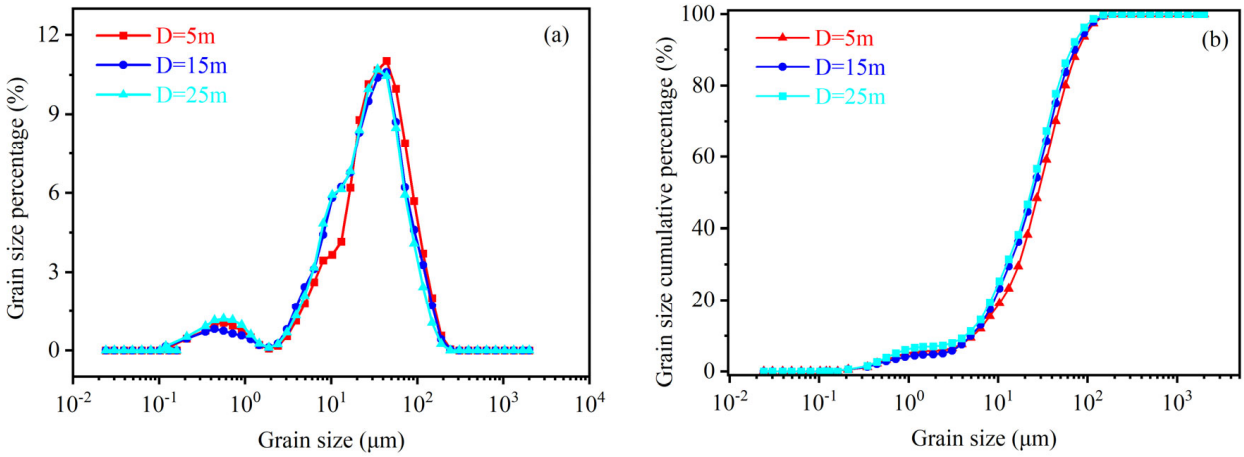

Figure 1. Grain distribution characteristics. (**a**) Grain size distribution curves; (**b**) grain size cumulative distribution curves.

2.2. SWCC Measurement

The wetting SWCC was determined using the filter paper method. Since the reliability of this method depends greatly on the meticulousness of the operators, and it is particularly sensitive to the handling of the samples, we chose to employ the Fredlund SWCC-150 pressure plate apparatus to measure the wetting SWCC. This allowed us to compare and verify the measuring procedures of the filter paper method. The Fredlund SWCC-150 pressure plate offers the advantage of capturing volume changes during the SWCC measurement process. In this experimental setup, the loess specimen, initially having a water content of 8%, was subjected to varying levels of air pressure, namely 500, 400, 300, 200, 100, 80, 60, 40, 20, 10, 6, and 2 kPa.

For the filter paper method, the protocols aligned with ASTM Standard D5298-10 [29]. The steps are outlined as follows: (i) Specimens were dried in an oven for 24 h initially. (ii) Specimens were incrementally wetted to specific water contents and sealed for 12 days, with water contents ranging from 3% to 30% (approximately 3% to 85% saturation). (iii) Three circular pieces of filter paper were employed, with the suction measuring filter paper (Whatman No. 42 filter paper) in the middle. The diameter of the suction-measuring filter paper was slightly smaller than that of the other two filter papers. Identical soil specimens sandwiched with the three pieces of filter paper were sealed together with tinfoil and wax and placed in a controlled 20 °C environment to minimize evaporation

and temperature fluctuations. (iv) After 14 days, the mass of the Whatman No. 42 filter paper was measured using a high-precision balance with a precision of 0.0001 g. The water content of the tested specimens was re-measured using the oven-drying method. The suction corresponding to the newly determined soil-water content was calculated using the calibration curve of the filter paper method recommended by ASTM D5298-10 [29].

2.3. Mercury Intrusion Method

The pore size distribution curves of the three soil samples were determined using mercury intrusion porosimetry. The testing procedure involved shaping the soil samples into cylindrical forms. Subsequently, the samples underwent freeze-drying to remove moisture without altering the soil pore structure. Following this, the soil samples were subjected to testing using an AutoPore IV 9500 (Micromeritics, Norcross, GA, USA) fully automated mercury intrusion porosimeter. This porosimeter can apply pressures ranging from 0 to 414 MPa and measure pore sizes within the range of 0.003 to 1000 μm.

3. Results

3.1. Soil Water Retention Curves

Figure 2 presents the results obtained from the pressure plate method. Figure 2a provides insight into the variation of void ratio during wetting as determined through the pressure plate method. In Figure 2b, two distinct data series are displayed: one is derived based on the initial void of the specimen, while the other incorporates modifications accounting for specimen deformation.

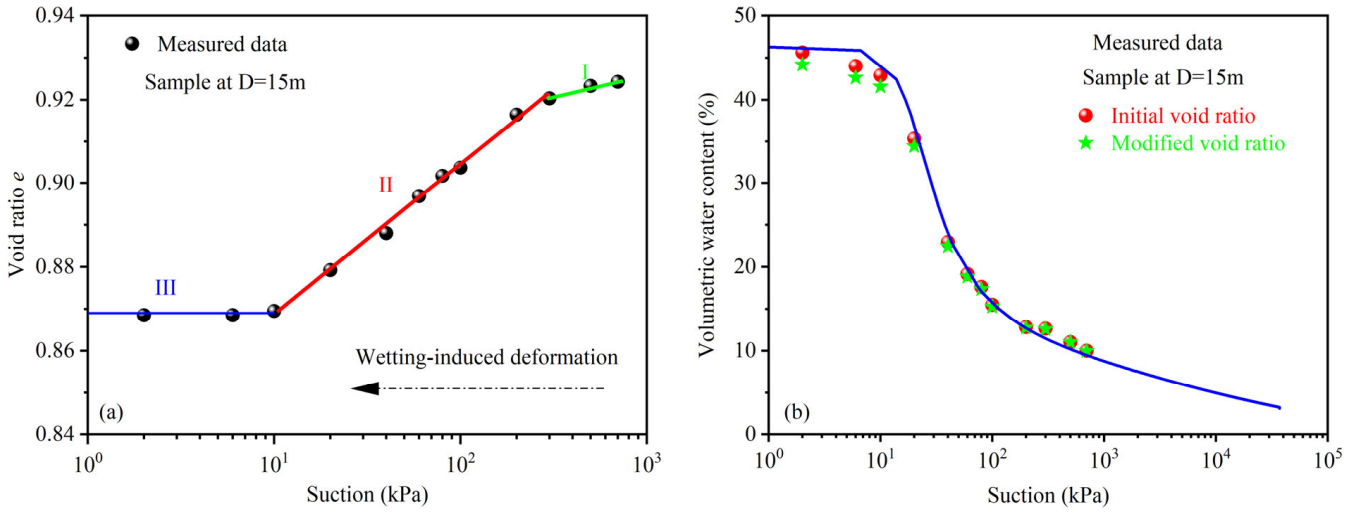

Figure 2. Deformation and soil water characteristics during wetting. (**a**) Wetting-induced deformation; (**b**) SWCC.

It is worth noting that loess, characterized by its open structure, exhibits a pronounced sensitivity to water and is prone to experiencing collapse deformation during wetting [5,30,31]. Figure 2a reveals that the soil underwent three stages of deformation during wetting. Initially, the deformation remained relatively limited, and subsequently it increased rapidly. While at near saturation (e.g., 0–10 kPa), minimal to no deformation was observed. These findings align with experimental data reported in prior studies [32–34]. Pereira and Fredlund [34] have elucidated that unsaturated soil typically undergoes three distinct stages of collapse: the pre-collapse stage, the collapse stage, and the post-collapse stage, in response to the decrease in suction. The pre-collapse stage is characterized by limited elastic volumetric deformation. The subsequent collapse phase is marked by significant volumetric compression in response to decreasing suction or increasing water content. This phase leads to notable alterations in soil structure due to localized shearing

of connecting bonds and clay aggregates. The post-collapse phase, manifesting at low suctions, is characterized by minimal to no volumetric deformation.

It is important to note that the overall variation in void ratio amounted to 0.06, which corresponded to a total strain of 6%. The impact of deformation during the test on the SWCC was constrained within the suction range exceeding 40 kPa. However, this influence became progressively more pronounced as suction decreased, as illustrated in Figure 2b.

Figure 3a presents a comparative analysis of the wetting SWCC data acquired through both the axis translation technique and the filter paper method for the specimen at a depth of D = 15 m. Notably, the data obtained from these distinct methods exhibit remarkable alignment. This consistency not only underscores the quality and validity of the filter paper method but also underscores the homogeneity of the specimens used in this study.

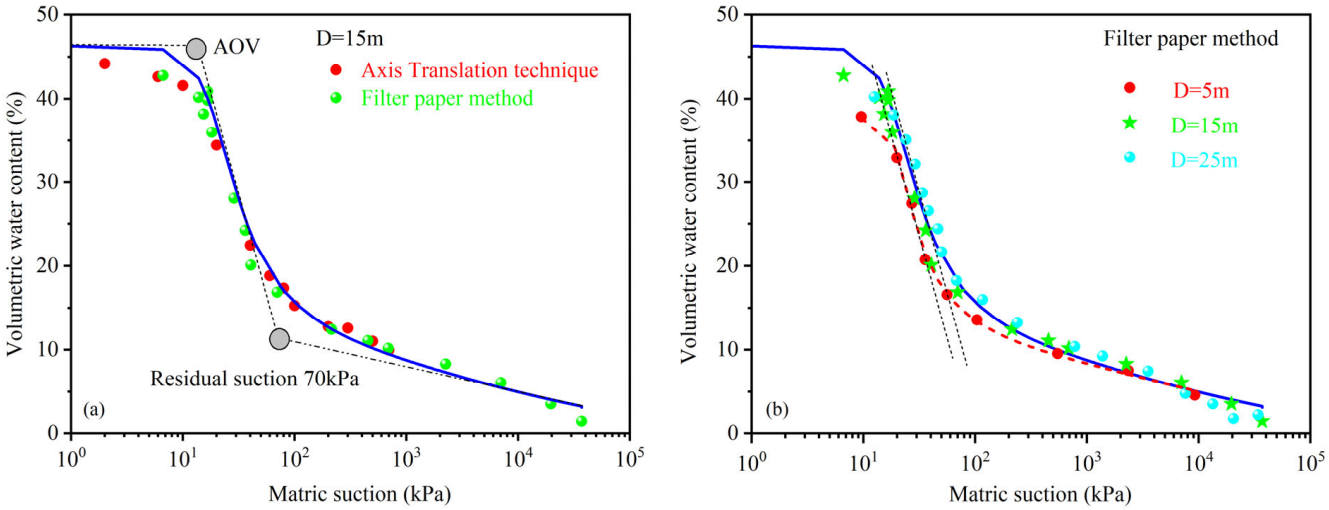

Figure 3. SWCC of the tested specimen. (**a**) Comparison between the axis translation technique and filter paper method in measuring the SWCC; (**b**) SWCCs of loess at different depths.

Vanapalli et al. [14] have proposed a categorization of the SWCC into three distinct zones based on critical values: the air entry suction value (AEV) for the drying process or the air occlusion value (AOV) for the wetting process, and the residual suction value (ψ_r). These three zones are the boundary effect zone with the suction ranging from 0 to AEV/AOV), the transition zone with the suction spanning from AOV to ψ_r, and the residual zone with the suction higher ψ_r. The determination of AEV/AOV and ψ_r can be accomplished using the method outlined by Vanapalli et al. [20]. Notably, for the D = 15 m specimen, the ψ_r value is determined to be 70 kPa, while the AOV is estimated at 15 kPa. It is evident that the influence of soil deformation on the SWCC predominantly manifests within the boundary effect zone.

Figure 3b provides a visual representation of the SWCC for samples obtained at varying depths. As the burial depth of the soil layer increased, the SWCC curve exhibited an extended near-saturation zone, accompanied by an increase in the AOV. Remarkably, the slope of the SWCC within the transition zone remained relatively consistent. This observation underscores the fact that the primary impact of burial depth lies in its influence on the AOV within the soil's SWCC.

3.2. Pore Size Distribution Data

The specimen located at a depth of D = 15 m experienced structural failure during testing, leading to the availability of data exclusively for depths of D = 5 m and D = 25 m. Figure 4 illustrates the pore size distribution (PSD) curve and the cumulative intruded volume curves of the specimens.

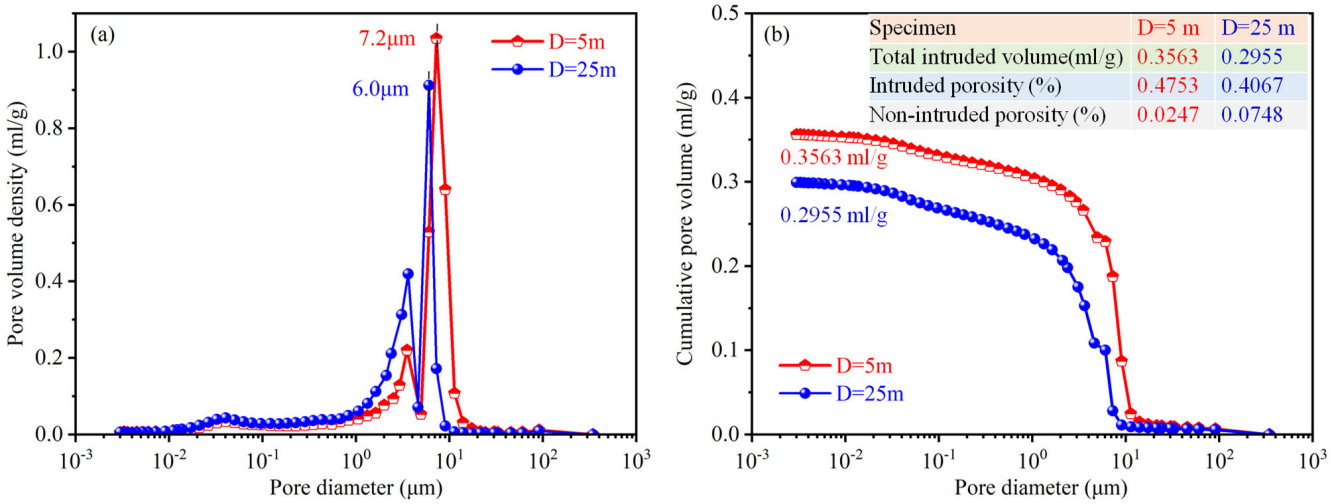

Figure 4. Pore characteristics. (**a**) Pore size distribution curves; (**b**) cumulative pore volume distribution curve.

The PSD curves for specimens at D = 5 m and D = 25 m exhibited a similar overall shape. The influence of burial depth primarily manifested within the pore size range of 1–15 μm. In the case of the D = 5 m specimen, the peak pore size was observed at 7.2 μm, with a corresponding pore density at the peak measuring 1.035 mL/g. In contrast, for the D = 25 m specimen, the peak pore size was slightly smaller at 6.0 μm, accompanied by a corresponding pore density of 0.912 mL/g. When examining pore sizes smaller than 1 μm and larger than 15 μm, the PSD curves for both depths essentially overlapped.

Figure 4b reveals a notable variation in the amount of mercury intrusion as the pore size decreased within the 1 to 15 μm range, signifying that the pores were predominantly within this size range. The total intrusion pore volumes measured were 0.3563 mL/g for the D = 5 m specimen and 0.2995 mL/g for the D = 25 m specimen. The corresponding porosity values for D = 5 m and D = 25 m were 0.4753 and 0.4076, respectively. The non-intruded porosity (the difference between total porosity and porosity measured by mercury intrusion) stood at 0.0247 and 0.0748 for D = 5 m and D = 25 m, respectively. It needs to be mentioned that mercury can only infiltrate connected pores within the sample and pores falling within the size range of 0.003 to 1000 μm. These findings suggest that the D = 25 m soil sample may possess a higher proportion of closed pores or an increased number of minuscule pores (d < 0.003 μm), contributing to the lower mercury intrusion observed in this case.

4. Discussion

The Young–Laplace equation (Equation (1)) serves as a functional link between soil pore diameter (d) and suction (ψ). As the size and distribution of pore diameter (d) are important indicators that characterize the microstructure of soil and the relationship between suction (ψ) and soil water content represents the SWCC, the Young–Laplace equation establishes a connection between the micro-pore structure of soil and the macro-scale soil-water properties.

$$u_a - u_w = \psi = \frac{4T_w \cos\theta}{d} \quad (1)$$

where u_w is the pore water pressure; u_a is the air pressure; ψ is the matric suction; T_w is the water-air interfacial tension with a value of 72.72×10^{-3} N/m at 20 °C; θ is the contact angle at the air-water-soil interface, which can be assumed to be 60° as suggested by Li et al. [35]; and d is the pore diameter corresponding to suction ψ.

By employing Equation (1) to convert pore sizes into their corresponding suctions, it became possible to establish a correlation analysis between the PSD and SWCC curves, as illustrated in Figure 5. These two curves exhibited a noticeable correspondence. This

alignment arose from the fact that pores within the dominant size range serve as the principal reservoirs for water storage. Even minor fluctuations in their quantity and distribution range can result in substantial variations in soil water content. Consequently, the dominant pore size range depicted in the PSD curve closely corresponded to the transitional region of the SWCC. In contrast, pores with lower distribution density store comparatively less moisture, and variations in the quantity and range of such pores exert a relatively modest influence on soil water content.

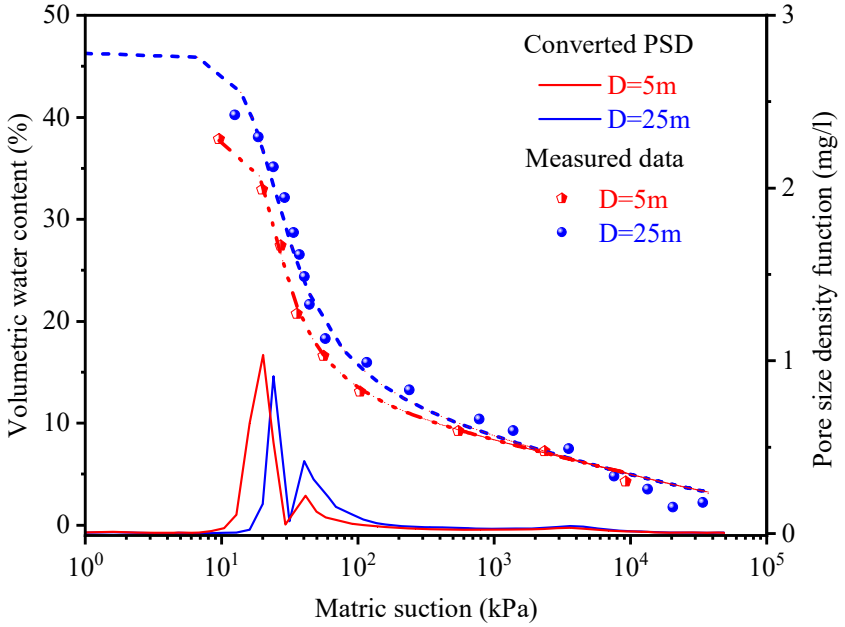

Figure 5. Relationship between the SWCC and PSD (converted to suction).

It is widely acknowledged that the process of forcing mercury into soil specimens closely resembles the soil drying process facilitated by the axis translation technique. Under external pressure, mercury tends to infiltrate large pores, whereas during the wetting process, water predominantly occupies small pores. These two fluids, water and mercury, essentially occupy complementary spaces within the soil. To calculate the volume of water intrusion (V_w) associated with a specific pore size, one simply subtracts the volume of mercury intrusion (V_m) from the total pore volume (V). Consequently, the soil's volumetric moisture content can be determined using Equation (2).

$$\theta_{\mathrm{w}} = (V_w / V_t) = (V - V_m)/V_t = n - V_m/V_t \quad (2)$$

θ_{w} is the volumetric water content; V is the total pore volume; V_w represents the water volume; V_m is the mercury intrusion volume at pore size d; n is the porosity; and V_t is the sum of the soil particles' volume and mercury-intruded pore volume.

V_m and V_t can be determined through the MIP test. The soil's SWCC can be derived by combining Equations (1) and (2). The findings are presented in Figure 6, which demonstrates a general alignment between the predicted results and the measured data over a wide suction range. However, it is noteworthy that the predicted results tended to overestimate the soil water content when the suction was less than 10 kPa. This discrepancy was more pronounced in the case of the D = 5 m specimen when compared to the deeper soil at a depth of D = 25 m. This variation may be attributed to wetting-induced soil deformation during the measurement of the SWCC, as illustrated in Figure 2.

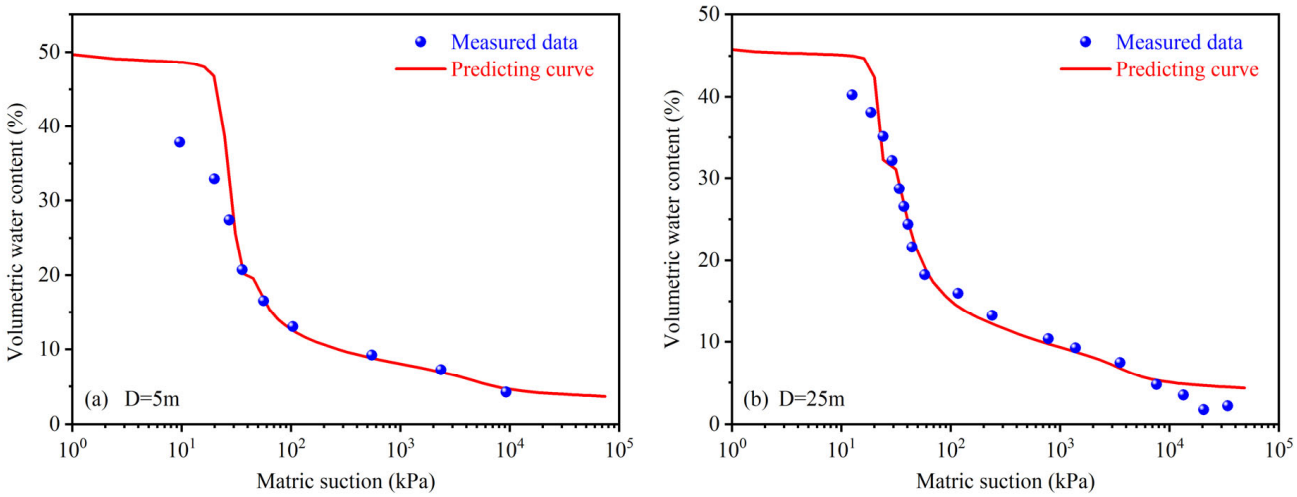

Figure 6. Comparison between the measured and predicted SWCC via the pore size data for the specimens at different depths.

It is important to note that water-retention behavior, especially within the residual suction range, is primarily influenced by adsorption, a phenomenon governed by the mineral composition of particles rather than capillarity [36]. This adsorption-dominated behavior has been well-established in prior research [37,38]. Consequently, suction values derived from pore size using the Young–Laplace equation in the high suction range may not accurately represent the actual suction conditions. However, it is intriguing to observe that the predicted curves exhibited a strong agreement with the measured data over a wide suction range (e.g., 10–10^4 kPa), including the residual suction range (e.g., >70 kPa), as depicted in Figure 6. This consistency is not coincidental, as similar findings have been reported by Hou et al. [39] and Li et al. [35]. One plausible explanation for this phenomenon may be attributed to the presence of non-intruded pores, whose volume was considered in the calculation of the wetting SWCC using the MIP data. Conversely, these non-intruded pores are typically disregarded when utilizing MIP data to predict the drying SWCC. In the drying process, soil water content approaches zero as suction increases towards the highest suction value of 10^6 kPa [24,27].

5. Summary and Conclusions

In this study, we investigated the SWCC and microstructure of intact specimens buried at varying depths. SWCC data were acquired using both the filter paper method and the axis translation technique, while microstructural analysis was performed using MIP. Our findings provide valuable insights into the influence of burial depth on SWCC and the characteristics of pore size distribution.

It is worth noting that at the study site, the soils buried at different depths exhibited similar grain compositions and fundamental physical properties, despite variations in dry density. Deeper soil burial led to a higher AOV and a comparable slope of the SWCC in the transition zone, in comparison to specimens at shallower depths. This transitional region of the SWCC corresponded to the dominant pore size range observed in the PSD curve. Predictions based on MIP data demonstrated robust performance for the wetting SWCC over a wide suction range (e.g., 10–10^4 kPa). However, it is important to acknowledge that the overestimation observed in MIP predictions can be attributed to wetting-induced soil deformation. These findings underscore the pivotal role of pore structure in governing soil water retention behavior.

Furthermore, it is crucial to emphasize that the grain compositions of specimens at various depths were nearly identical, as were their fundamental physical properties. The variation in burial depth primarily contributed to differences in dry density and pore structure. This observed influence of burial depth on the SWCC aligns with the

influence of dry density, as in the findings reported by Wang et al. [22], Hu et al. [17], and Gao and Sun [16]. However, it is imperative to recognize that significant variations in SWCC and PSD may occur when soils at different depths belong to distinct types (e.g., silt loess, paleosol).

Author Contributions: Conceptualization, methodology, investigation, visualization, writing, and funding acquisition, X.H.; Conceptualization, writing—review and editing, and funding acquisition, S.Q.; visualization, F.L. All authors have read and agreed to the published version of the manuscript.

Funding: This research was supported by the Strategic Priority Research Program of the Chinese Academy of Sciences, Grant No. XDA23090402, and the National Natural Science Foundation of China under Grant Nos. 42107188, 42141009.

Data Availability Statement: All relevant data are available from the corresponding author by request.

Acknowledgments: Additional thanks are given to Tonglu Li, Ping Li, Quanli Zhao, and Shuang Wu for the help in sampling and conducting the experiment.

Conflicts of Interest: The authors declare no conflict of interest.

References

1. Gao, L.; Shao, M. The interpolation accuracy for seven soil properties at various sampling scales on the Loess Plateau, China. *J. Soils Sediments* **2012**, *12*, 128–142. [CrossRef]
2. Yao, X.; Fu, B.; Lü, Y.; Chang, R.; Wang, S.; Wang, Y.; Su, C.H. The multiscale spatial variance of soil moisture in the semi-arid Loess Plateau of China. *J. Soils Sediments* **2012**, *12*, 694–703. [CrossRef]
3. Barden, L.; McGown, A.; Collins, K. The collapse mechanism in partly saturated soil. *Eng. Geol.* **1973**, *7*, 49–60. [CrossRef]
4. Feda, J. Collapse of loess upon wetting. *Eng. Geol.* **1988**, *25*, 263–269. [CrossRef]
5. Hou, X.K.; Vanapalli, S.K.; Li, T.L. Wetting-induced collapse behavior associated with infiltration: A case study. *Eng. Geol.* **2019**, *258*, 105146. [CrossRef]
6. Tu, X.B.; Kwong, A.K.L.; Dai, F.C.; Tham, L.G.; Min, H. Field monitoring of rainfall infiltration in a loess slope and analysis of failure mechanism of rainfall-induced landslides. *Eng. Geol.* **2009**, *105*, 134–150. [CrossRef]
7. Ma, L.N.; Qi, S.W.; Zheng, B.W.; Guo, S.F.; Huang, Q.B.; Yu, X. Farming Influence on Physical-Mechanical Properties and Microstructural Characteristics of Backfilled Loess Farmland in Yan'an, China. *Sustainability* **2020**, *12*, 5516. [CrossRef]
8. Hou, X.; Li, T.; Vanapalli, S.K.; Xi, Y. Water percolation in a thick unsaturated loess layer considering the ground-atmosphere interaction. *Hydrol. Process.* **2019**, *33*, 794–802. [CrossRef]
9. Huang, T.M.; Ma, B.; Pang, Z.; Li, Z.; Li, Z.; Long, Y. How does precipitation recharge groundwater in loess aquifers? Evidence from multiple environmental tracers. *J. Hydrol.* **2020**, *583*, 124532. [CrossRef]
10. Li, P.; Li, T.L.; Vanapalli, S.K. Influence of environmental factors on the wetting front depth: A case study in the Loess Plateau. *Eng. Geol.* **2016**, *214*, 1–10. [CrossRef]
11. Wang, C.X.; Li, T.L.; Li, P.; Wang, Y.; Li, H.; Xi, Y. Verification on the mode of moisture transfer in the vadose zone of thick loess. *Hydrol. Process.* **2022**, *36*, e14656. [CrossRef]
12. Zhang, C.L.; Li, T.L.; Li, P. Rainfall infiltration in Chinese loess by in situ observation. *J. Hydrol. Eng.* **2014**, *19*, 06014002. [CrossRef]
13. Fredlund, D.G.; Xing, A. Equations for the soil-water characteristic curve. *Can. Geotech. J.* **1994**, *31*, 521–532. [CrossRef]
14. Vanapalli, S.K.; Fredlund, D.G.; Pufahl, D.E.; Clifton, A.W. Model for the prediction of shear strength with respect to soil suction. *Can. Geotech. J.* **1996**, *33*, 379–392. [CrossRef]
15. Zhai, Q.; Rahardjo, H. Estimation of permeability function from the soil-water characteristic curve. *Eng. Geol.* **2015**, *199*, 148–156. [CrossRef]
16. Gao, Y.; Sun, D.A. Soil-water retention behavior of compacted soil with different densities over a wide suction range and its prediction. *Comput. Geotech.* **2017**, *91*, 17–26. [CrossRef]
17. Hu, R.; Chen, Y.F.; Liu, H.H.; Zhou, C.B. A water retention curve and unsaturated hydraulic conductivity model for deformable soils: Consideration of the change in pore-size distribution. *Geotechnique* **2013**, *63*, 1389–1405. [CrossRef]
18. Van Genuchten, M.T. A closed-form equation for predicting the hydraulic conductivity of unsaturated soils 1. *Soil Sci. Soc. Am. J.* **1980**, *44*, 892–898. [CrossRef]
19. Yang, H.; Rahardjo, H.; Leong, E.C.; Fredlund, D.G. Factors affecting drying and wetting soil-water characteristic curves of sandy soils. *Can. Geotech. J.* **2004**, *41*, 908–920. [CrossRef]
20. Vanapalli, S.K.; Fredlund, D.G.; Pufahl, D.E. The influence of soil structure and stress history on the soil-water characteristics of a compacted till. *Géotechnique* **1999**, *49*, 3–159. [CrossRef]
21. Simms, P.H.; Yanful, E.K. Predicting soil-water characteristic curves of compacted plastic soils from measured pore-size distributions. *Géotechnique* **2002**, *52*, 69–278. [CrossRef]

22. Wang, Y.; Li, T.L.; Zhao, C.X.; Hou, X.K.; Li, P.; Zhang, Y. A study on the effect of pore and particle distributions on the soil water characteristic curve of compacted loess soil. *Environ. Earth Sci.* **2021**, *80*, 764. [CrossRef]
23. Han, Z.; Vanapalli, S.K.; Zou, W.L. Simple approaches for modeling hysteretic soil water retention behavior. *J. Geotech. Geoenviron. Eng.* **2019**, *145*, 04019064. [CrossRef]
24. Otalvaro, I.F.; Neto, M.P.C.; Delage, P.; Caicedo, B. Relationship between soil structure and water retention properties in a residual compacted soil. *Eng. Geo.* **2016**, *205*, 73–80. [CrossRef]
25. Romero, E.; Della Vecchia, G.; Jommi, C. An insight into the water retention properties of compacted clayey soils. *Géotechnique* **2011**, *61*, 313. [CrossRef]
26. Poulovassilis, A.; Childs, E.C. The hysteresis of pore water: The non-independence of domains. *Soil Sci.* **1971**, *112*, 301–312. [CrossRef]
27. Muñoz-Castelblanco, J.A.; Pereira, J.M.; Delage, P.; Cui, Y.J. The water retention properties of natural unsaturated loess from northern France. *Géotechnique* **2012**, *62*, 95. [CrossRef]
28. Ng, C.W.W.; Sadeghi, H.; Belal Hossen, S.B.; Chiu, C.F.; Alonso, E.E.; Baghbanrezvan, S. Water retention and volumetric characteristics of intact and re-compacted loess. *Can. Geotech. J.* **2016**, *53*, 1258–1269. [CrossRef]
29. *ASTM Standard D5298-10*; Standard Test Method for Measurement of Soil Potential (Suction) Using Filter Paper. ASTM International: West Conshohocken, PA, USA, 2006.
30. Xie, W.L.; Li, P.; Zhang, M.S.; Cheng, T.E.; Wang, Y. Collapse behavior and microstructural evolution of loess soils from the Loess Plateau of China. *J. Mt. Sci.* **2018**, *15*, 1642–1657. [CrossRef]
31. Wei, Y.N.; Fan, W.; Yu, B.; Deng, L.S.; Wei, T. Characterization and evolution of three-dimensional microstructure of Malan loess. *Catena* **2020**, *192*, 104585. [CrossRef]
32. Garakani, A.A.; Haeri, S.M.; Khosravi, A.; Habibagahi, G. Hydro-mechanical behavior of undisturbed collapsible loessial soils under different stress state conditions. *Eng. Geol.* **2015**, *195*, 28–41. [CrossRef]
33. Jotisankasa, A.; Ridley, A.; Coop, M. Collapse behavior of compacted silty clay in suction-monitored oedometer apparatus. *J. Geotech. Geoenviron. Eng.* **2007**, *133*, 867–877. [CrossRef]
34. Pereira, J.H.; Fredlund, D.G. Volume change behavior of collapsible compacted gneiss soil. *J. Geotech. Geoenviron. Eng.* **2000**, *126*, 907–916. [CrossRef]
35. Li, H.; Li, T.L.; Li, P.; Zhang, Y.G. Prediction of loess soil-water characteristic curve by mercury intrusion porosimetry. *J. Mt. Sci.* **2020**, *17*, 2203–2213. [CrossRef]
36. Lu, N.; Likos, W.J. *Unsaturated Soil Mechanics*; John Wiley and Sons: Hoboken, NJ, USA, 2004.
37. Frydman, S.; Baker, R. Theoretical soil-water characteristic curves based on adsorption, cavitation, and a double porosity model. *Int. J. Geomech.* **2009**, *9*, 250–257. [CrossRef]
38. Tuller, M.; Or, D. Water films and scaling of soil characteristic curves at low water contents. *Water Resour. Res.* **2005**, *41*, W09403. [CrossRef]
39. Hou, X.K. Prediction of the loess's soil water retention curve using the pore data from the mercury intrusion technique. *Water* **2023**, *15*, 3273. [CrossRef]